Title

Carbon Dioxide Dimer Radical Anion as Surface Intermediate of Photoinduced CO2 Reduction at Aqueous Cu and CdSe Nanoparticle Catalysts by Rapid-Scan FT-IR Spectroscopy

Journal

Journal of the American Chemical Society, 140(12)

ISSN

0002-7863

Authors

Sheng, Hua
Oh, Myoung Hwan
Osowiecki, Wojciech T
et al.

Publication Date

2018-03-28

DOI

10.1021/jacs.8b00271

Peer reviewed

Carbon Dioxide Dimer Radical Anion as Surface Intermediate of Photo-induced CO_2 Reduction at Aqueous Cu and CdSe Nanoparticle Catalysts by Rapid-Scan FT-IR Spectroscopy

H. Sheng[a], M. Oh[b,c], W. T. Osowiecki[b,c], W. Kim[d], A. P. Alivisatos[b,c,e,f], H. Frei[a*]

[a]Molecular Biophysics and Integrated Bioimaging Division, Lawrence Berkeley National Laboratory, Berkeley, CA 94720

[b]Materials Sciences Division, Lawrence Berkeley National Laboratory, Berkeley, CA 94720

[c]Department of Chemistry, University of California, Berkeley, CA 94720

[e]Department of Materials Science and Engineering, University of California, Berkeley, CA 94720

[f]Kavli Energy NanoScience Institute, Berkeley, CA 94720

(*J. Am Chem. Soc.*, accepted)

[d] Current address: Dept. of Chemical and Biological Engineering, Sookmyung Women's University, Seoul, 04310 Korea

Abstract

Monitoring of visible light sensitized reduction of CO_2 at Cu nanoparticles in aqueous solution by rapid-scan ATR FT-IR spectroscopy on the time scale of seconds allowed structural identification of a one-electron intermediate and demonstrated its kinetic relevancy for the first time. Isotopic labelling (^{12}C: 1632, 1358, 1346 cm^{-1}; ^{13}C: 1588, 1326, 1316 cm^{-1}) revealed a species of carbon dioxide dimer radical anion structure, most likely bound to the catalyst surface through carbon. Intermediacy of Cu-C(=O)OCO_2^- surface species is in agreement with a recently proposed mechanism for eletrocatalytic CO_2 reduction at Cu metal nanoparticles based on Tafel slope analysis. Spontaneous decrease of the intermediate after termination of the photosensitization pulse (Sn porphyrin excited at 405 nm) was accompanied by the growth of HCO_3^-. CO was produced as well, but sensitive detection required photolysis for tens of minutes. A direct kinetic link between a $C_2O_4^-$ surface intermediate and the CO product was also demonstrated for photocatalyzed CO_2 reduction at aqueous CdSe nanoparticles, where first order growth of a Cd-C(=O)OCO_2^- species was accompanied by rise of CO and HCO_3^- showing a distinct induction period. Fast detection of the CO was made possible by use of a Ni complex acting as efficient CO trap. The detection of the one-electron surface intermediate and confirmation of its catalytic relevancy was enabled by the delivery of electrons one-by-one by the photosensitization method, which in turn allowed manipulation of buildup and lifetime of the intermediate. The observation of carbon dioxide dimer radical anion points to approaches for rate enhancements of heterogeneous CO_2 reduction by creating catalytic environments that favor formation of this intermediate.

1. Introduction

Photo- and electrocatalytic reduction of carbon dioxide is of intense current interest because of the potential of generating energy-dense fuels.[1-3] For heterogeneous approaches, Cu electrodes play a unique role because the metal affords energy-dense products such as methane, ethylene, or ethanol beyond the formation of two-electron reduction products CO or formic acid.[4-7] Substantial progress in enhancing activity and product selectivity of Cu based catalysts has been achieved in the past few years through the development of thermal and electrochemical pretreatment methods,[8,9] use of bimetallic materials,[10,11] nanostructuring,[12,13] or a combinations thereof.[14] However, understanding of the detailed catalytic mechanisms responsible for the observed enhancement of activity or selectivity, in particular for aqueous systems, is very limited. Most mechanistic proposals are based on Tafel plot analyses, order dependence of product current on reactant concentrations, and on DFT computational studies.[4-7,15-19] Identification of detected surface species by structure specific spectroscopy combined with monitoring of the kinetic behavior for assessing catalytic relevancy is currently lacking.

Infrared spectroscopy in the attenuated total reflection mode, surface-enhanced infrared absorption spectroscopy, and laser sum frequency generation techniques have been used by several groups for in situ monitoring of electrocatalytic CO_2 reduction at metal electrodes.[20-28] Surface enhanced Raman spectroscopy has also been utilized for in situ probing of electrocatalytic CO_2 reduction.[29] In these reports, infrared bands of carbon dioxide radical anion (CO_2^-) or its protonated form (COOH) have been proposed,[4,24,27] including for systems using Cu metal catalysts.[28,30] Vibrational modes of these one-electron intermediates are expected to absorb in the same spectral region as stable carbonate or bicarbonate species in various surface adsorbed configurations, rendering structural identification very challenging. It

requires structure specific information based on isotopic ^{13}C and D labeling combined with knowledge of the kinetic behavior by temporally resolved spectroscopy to establish catalytic relevancy and role in the cycle. However, steady-state infrared studies reported todate lack this information. Furthermore, band assignments for proposed intermediates in these studies are based on literature data for closed shell molecules such as carboxylates instead of relevant open shell species.

Here, we report monitoring of visible light sensitized CO_2 reduction at the aqueous Cu nanoparticle interface by rapid-scan FT-IR spectroscopy in the attenuated total reflection configuration (ATR). A parallel study on aqueous CdSe photocatalyst nanoparticles provided crucial insights that complemented observations on the Cu system. The precise temporal control of electron delivery to the catalyst by photo-initiation allows us to unravel the kinetics of spontaneous reactions of surface intermediates and therefore to establish the catalytic relevancy of the observed species and to identify their role in the reduction cycle.

2. Experimental

Chemicals: CdSe quantum dots with 3-mercaptopropionic acid (MPA) as stabilizer were prepared by the reaction of Cd^{2+} with NaHSe as reported previously.[31] The size of the quantum dots and the concentration of the colloid were determined by UV-Vis spectroscopy according to a method reported by Peng [32] (Figure S1). The water-soluble photosensitizer, $Sn^{IV}(TPy^{H}P)(H_2O)_2(NO_3)_6$ (abbrev. SnP, Figure 1; $TPy^{H}P$ = protonated *trans*-dihydroxo[5,10,15,20-tetra(4-pyridyl)-porphyrinato]tin(IV)) and the chemical trap for evolving CO, $Ni^{II}(TMC)Cl_2$ (TMC =

1,4,8,11-tetramethyl-1,4,8,11-tetraazacyclotetradecane) were synthesized according to the literature.[33,34] Cadmium(II) chloride, tin(IV) chloride, nickel (II) chloride hexahydrate, selenium powder, sodium borohydride, MPA, TPyP, TMC, sodium L-ascorbate, dehydroascorbic acid, trimethylamine (TEA), diethylamine (DEA), diethylamine-d_{10} (98 atom% D) and carbon dioxide-^{13}C (99 atom% ^{13}C, < 3 atom% ^{18}O) were purchased from Sigma-Aldrich and used as received. Deuterium oxide (D, 99.96%) was purchased from Cambridge Isotope Laboratories.

Synthesis of copper nanoparticles: For the preparation of Cu nanocrystals, 0.341 g (2 mmol) of copper(II) chloride (Aldrich) and 0.845 g (4.8 mmol) of ascorbic acid was dissolved in 30 mL of methylformamide (Aldrich) in a 100 mL flask equipped with a reflux condenser. The reaction mixture was stirred under purging with argon at room temperature for 30 min and heated to 90 °C for 12 h. The solution was cooled to room temperature and mixed with 70 mL of ethyl acetate to flocculate Cu nanocrystals. Cu nanocrystals were recovered by centrifugation and repeatedly purified by dispersing in water and precipitating with tetrahydrofuran. TEM imaging showed particles of between 2 and 3 nm diameter, consistent with the absence of visible plasmon absorption that indicates particle size smaller than 5 nm.[35] When exposed to air, the brown particle color did not turn greenish as would be the case if oxidation had resulted in the formation of Cu^{II}. At the same time, the presence of some Cu^{I} surface sites was indicated by the observation of the characteristic CO infrared band at 2113 cm^{-1} [36] when bubbling CO gas through an aqueous colloidal particle solution. This band disappeared upon visible light

photosensitization of the Cu particles due to re-reduction to Cu^0, which binds CO molecules more weakly than Cu^I.

Transient optical absorption spectroscopy: To verify electron transfer between reduced $SnP^{\bullet-}$ sensitizer and Cu nanoparticles, a nanosecond transient absorption spectrometer, Edinburgh Instruments model LP920, equipped with a pulsed Xe probe lamp was used in conjunction with a Nd:YAG laser-pumped tunable optical parametric oscillator (Continuum model Surelite II and Surelite OPO Plus) as the excitation source. The laser pulse width was 8 ns and measurements were conducted at 1 Hz repetition rate. In typical experiments, aqueous solutions in a quartz cuvette of 1 cm path length containing 50 μM SnP with varying concentrations of trimethylamine electron donor (0.1 to 0.3 M) and Cu nanoparticles (0 to 20 g/L) were purged with nitrogen and illuminated at 550 nm (10 mJ/pulse).

Rapid-scan FT-IR spectroscopy of photocatalytic reactions: A FT-IR spectrometer Bruker model Vertex 80 equipped with HgCdTe PV detector (Kolmar Technologies model KMPV11-1-J2, 14 μm band gap) was used. Rapid-scan spectra were recorded in double-sided/forward-backward mode with mirror velocity of 160 kHz and spectral resolution of 4 cm^{-1}. The visible light source for the photocatalytic reaction was a Spectra Physics continuous wave diode laser emitting at 405 nm (200 mW max. power). Light pulses were generated by intercepting the laser beam by a mechanical shutter with variable opening times from 0.3 ms to continuous (Vincent Associates model Uniblitz controlled by a BNC pulse/delay generator model 565). For precise

synchronization of photolysis pulse and spectral data acquisition, opening of the shutter was triggered by the forward motion of the FT-IR interferometer mirror.

For rapid-scan ATR FT-IR experiments, a ten-reflection diamond ATR accessory Harrick model ConcentratIR2 was used. The infrared beam path inside the accessory and the rest of the sample compartment was held under N_2 flow to avoid atmospheric water and CO_2 absorption. In a typical measurement, 15 μL aqueous colloidal solution was placed on the surface of the diamond element. A home-made cylindrical Teflon enclosure for controlling the gas phase of the headspace above the liquid sample was installed and sealed against the ATR support plate by an O-ring. The enclosure featured gas line connections for the supply of CO_2 or Ar (1 atm). A quartz window at the top of the enclosure allowed entry of the photolysis laser beam normal to the ATR plate. To remove oxygen and saturate the colloidal solution with CO_2 prior to start of photocatalysis, Ar flow was applied for 8 min followed by CO_2 flow for 1 min. According to the growth behavior of the 2340 cm^{-1} infrared absorption of CO_2 dissolved in water, a period of 15 min was required for gas phase CO_2 to diffuse into the liquid and reach equilibrium, including equilibration with bicarbonate species generated by introduction of CO_2. FT-IR data were recorded in rapid-scan mode during 405 nm photosensitization as well as subsequent dark periods. Samples were replaced with fresh ones after each single photolysis period/subsequent dark period, and typically the results of eight experiments were averaged for further signal-to-noise improvement. To compensate for minor baseline distortion caused by laser illumination, FT-IR data were also collected for pure water samples using identical illumination conditions and measurement protocol. Baseline correction was performed by subtracting the latter spectra from the ones recorded during photocatalysis.

FT-IR detection of CO product: To detect CO generated in SnP photosensitized Cu nano-catalyst system, 4.5 mL aqueous solution which contained 0.1 mM SnP, 1 g/L Cu nanocrystals and 0.1 M TEA was prepared in a 10 mL Schlenk flask, which was connected to an infrared gas cell equipped with CaF_2 windows held under vacuum. The solution in the Schlenk flask was purged with Ar gas for 20 min and CO_2 for 1 min, after which 45 μL additional TEA was introduced to compensate for the amine consumed by evaporation or by protonation upon admission of CO_2. The solution was irradiated with 514 nm laser emission of the Ar ion laser Coherent model Innova 90C at 1.9 W for 5 h, with the beam expanded to a diameter of 3 cm in order to fully illuminate the flask. The gas content of the solution head-space was released into the infrared cell for recording of FT-IR gas spectra at 0.5 cm^{-1} resolution.

For the CdSe system, the efficient CO trap $Ni^{II}(TMC)Cl_2$ was employed for rapid detection of CO on the second time scale.[37] To prepare the sample, 5 mM $Ni^{II}(TMC)Cl_2$ was added to an aqueous solution of 0.4 mM CdSe nanoparticles and 0.1 M ascorbate. Because the region 2400 – 1900 cm^{-1} is opaque for diamond ATR elements, a 25 μm path-length CaF_2 transmission liquid cell was used for experiments with the $Ni^{II}(TMC)Cl_2$ trap. 1.5 mL of CdSe sample was purged with argon and carbon dioxide in a 4 mL vial before transfer to the CaF_2 liquid cell in a N_2 glovebox.

3. Results

3.1 Visible light photosensitized CO_2 reduction at aqueous Cu nanocrystals

To verify efficient electron injection into aqueous Cu nanocrystals by the visible light sensitizer SnP, nanosecond transient absorption spectroscopy was used to monitor quenching of visible light generated $SnP^{\bullet-}$ (Sn porphyrin radical anion) by the Cu particles in aqueous solution (ε_{red} = -0.87 V). Excitation of SnP with an 8 ns pulse at 550 nm in the presence of TEA donor generates an excited state that is quenched on the nanosecond time scale by the electron donor to yield the long-lived $SnP^{\bullet-}$ radical anion with an absorbance maximum around 700 nm (Figure 2a).[38] Electron transfer to Cu nanoparticles is manifested by increasing rate of decay of the $SnP^{\bullet-}$ signal as function of Cu particle concentration (Figure 2b). For a typical Cu concentration of 1.5 g/L used in the photocatalytic experiments, the decay traces show that $SnP^{\bullet-}$ is consumed quantitatively by electron transfer to Cu particles in less than 5 ms, which is short on the time scale of the rise of catalytic intermediates.

Confirmation of CO generation upon prolonged visible light sensitization at 514 nm of aqueous Cu particles was obtained by monitoring the gas content of the headspace of a solution containing 0.1 mM SnP, 1g/L Cu and 0.2 M TEA by FT-IR spectroscopy. To this end, the headspace of the evolving gas included a miniature infrared gas cell in the FT-IR sample compartment. As shown in Figure 3, the ro-vibrational bands of carbon monoxide reflecting the ^{12}C versus ^{13}C isotopic composition of the reacting CO_2 are observed as the sole gas phase product. Monitoring of CO product by fast chemical trapping on a much shorter time scale of seconds was not feasible with these samples because the efficient carbon monoxide trap $Ni(TMC)^{2+}$ was found to rapidly precipitate in the presence of Cu particles.

For photosensitization experiments with rapid-scan ATR FT-IR spectroscopy, laser emission at 405 nm instead of 514 nm was used because optical absorption of SnP at 405 nm is

six times higher than at the green wavelength.[38] This allowed us to reduce the laser intensity for photosensitization, which proved important for minimizing baseline distortions due to slight heating of the ATR setup during illumination. Most experiments were conducted in D_2O solution in order to allow monitoring of the critical 1600 – 1700 cm^{-1} region otherwise blocked by the H_2O bending mode. Rapid-scan spectra of Cu nanoparticles in $^{12}CO_2$ saturated D_2O recorded for a period of 20 s illumination show growth of bands centered at 1632, 1608, 1419, and 1360 cm^{-1}, as can be seen in Figure 4a. The 1632 and 1360 cm^{-1} bands shift to 1588 and 1330 cm^{-1}, respectively, when conducting the experiment with $^{13}CO_2$, indicating that this pair of absorptions originates from species produced by CO_2 reduction (Figure 4b). The 1608 cm^{-1} band does not exhibit a ^{13}C shift as it originates from the NH bending mode of protonated TEA.[39]

Closer inspection of the infrared absorption centered at 1360 cm^{-1} for $^{12}CO_2$, Figure 4c, reveals that the shape of the band profile changes during the initial 10 s of photolysis, indicating contribution of more than one species. Spectral deconvolution gives 3 components with peaks at 1368, 1358, and 1346 cm^{-1}. Analysis of the corresponding absorption for the $^{13}CO_2$ experiment around 1330 cm^{-1} reveals components centered at 1335, 1326 and 1316 cm^{-1}. The 1368 (^{12}C) and 1335 cm^{-1} (^{13}C) component in the photolysis spectra Figure 4c and 4d (marked blue) is in exact agreement with authentic spectra of bicarbonate species $D^{12}CO_3^-$ and $D^{13}CO_3$, respectively (Figure S2). Because the relative intensity of the pair of bands at 1358 and 1346 cm^{-1} for ^{12}C (1326 and 1316 cm^{-1} for ^{13}C counterpart, red traces) remains unchanged within uncertainties during the growth period, we propose that they belong to a single yet to be identified species. Both bands exhibit frequency and ^{13}C isotope shifts indicative of symmetric CO stretch modes, with the corresponding asymmetric CO stretch absorption at 1632 cm^{-1} (1588 cm^{-1} for ^{13}C modification). As shown in Figure S3, identical frequencies for these bands were observed in

H_2O solution, indicating that the species does not feature H atoms. Most notable is the absence of a large, 300 cm^{-1} red shift of a COH mode upon D substitution as observed for bicarbonate-H (δ(COH) at 1302 cm^{-1} (Figure S2)) versus bicarbonate-D (δ(COD) at 1025 cm^{-1}) that otherwise would indicate a protonated form of the intermediate.[40]

Crucial insight was gained by continued monitoring of infrared spectra under dark conditions following a brief photosensitization period. Spectral traces of the 1400 – 1300 cm^{-1} region recorded at 12, 20, 30, and 60 s after termination of photolysis are shown in the top part of Figure 5a and 5b for experiments with $^{12}CO_2$ and $^{13}CO_2$, respectively. Comparison of spectra before and after the 136 s dark period, presented in Figure 5c and 5d as blue (top) and red (bottom) traces for the $^{12}CO_2$ and $^{13}CO_2$ sample, respectively, indicate a spontaneous process resulting in frequency shifts of the band to higher values by 7-8 cm^{-1}. The final spectra at 136 s agree well with those of authentic samples of bicarbonate $D^{12}CO_3^-$ (1367 cm^{-1}) and $D^{13}CO_3^-$ (1335 cm^{-1}), respectively (shown as dotted traces) as can be seen from authentic bicarbonate spectra given in Figure S2. This observation suggests that the spontaneous dark process following photo-induced growth of bands at 1368, 1358, and 1346 cm^{-1} ($^{12}CO_2$) and at 1335, 1326 and 1316 cm^{-1} ($^{13}CO_2$) converts the species absorbing at 1358 and 1346 cm^{-1} (1326 and 1316 cm^{-1} for $^{13}CO_2$) to bicarbonate. This is borne out by the good agreement of the corresponding spectral deconvolution of the observed difference spectrum at 136 s dark period shown in the bottom traces of Figure 5a ($^{12}CO_2$) and 5b ($^{13}CO_2$); the superposition of the decreasing intermediate components (red) with the increasing bicarbonate band (blue) matches well with the observed difference spectrum (black trace). Because CO is detected after prolonged photosensitization of the Cu particles (Figure 3), these observations suggest that bicarbonate is the coproduct of CO, formed by spontaneous disproportionation of a one-electron surface intermediate. Nevertheless,

without the ability to monitor CO growth on the same time scale as the observed intermediate, the data of these experiments are insufficient for confirming the kinetic link. Such a link was provided by the study of CO_2 reduction photocatalyzed by aqueous CdSe particles (Sect. 3.2).

We can conceive of two structures for one-electron intermediates of CO_2 reduction that do not feature a hydrogen atom, namely CO_2^- (carbon dioxide radical anion) and $C_2O_4^-$ (carbon dioxide dimer radical anion), which is the adduct of CO_2^- and a second CO_2 molecule by forming a C-O bond (note: $C_2O_4^-$ designates O=C-O-CO_2^- structure throughout this paper; no occurrence of O_2C-CO_2^- is implied because oxalate is not observed as a product). For Cu catalysts, CO_2^- is the most frequently proposed one-electron surface intermediate,[4] while $C_2O_4^-$ has also been proposed to play a mechanistic role in electrocatalytic CO_2 reduction in aqueous [15,41] and non-aqueous solutions based on electrochemical observations.[4,42-47] For chalcogenide photocatalysts, $C_2O_4^-$ has been postulated as an intermediate of CO_2 reduction at CdS and ZnS nanocrystals.[48,49] A catalytic role of $C_2O_4^-$ is plausible in light of the fact adduct formation of CO_2^- with CO_2 is estimated to stabilize the CO_2^- species by 20 kcal mol^{-1}.[50]

A more detailed look at the observed infrared modes further supports the intermediacy of $C_2O_4^-$. CO_2^-, as a triatomic molecule, has three vibrational degrees of freedom that include an asymmetric and a symmetric stretch mode. Infrared spectra of CO_2^- generated in a solid neon gas matrix at cryogenic temperature show an asymmetric stretch around 1650 cm^{-1} with a ^{13}C shift of 42 cm^{-1}, and a symmetric stretch at 1254 cm^{-1} with a ^{13}C shift of 16 cm^{-1}.[51] The small ^{13}C shift of the symmetric stretch is characteristic for a carbon bound to two (instead of three) oxygens atoms, as also observed for other species such as O_2C-CO_2^-, which has an 8 cm^{-1} infrared ^{13}C shift for this mode.[52] Surface-enhanced Raman measurement of CO_2^- on Cu surface at 40 K reveals a symmetric stretch mode at 1182 cm^{-1}.[53] Very similar position for this mode of surface

absorbed CO_2^- at low temperature is observed by HREELS for other metals as well, e.g. at 1130 cm^{-1} for Ni or at 1232 cm^{-1} for Fe.[50,54] These reported frequencies and ^{13}C isotope shifts for CO_2^- species do not agree with spectral observations for our system, which include an asymmetric stretch at 1632 cm^{-1} with a ^{13}C shift of 44 cm^{-1} and two bands in the 1300-1400 cm^{-1} region, each with a ^{13}C shift between 30 and 32 cm^{-1}. In fact, three stretch modes in the 1000-1700 cm^{-1} region, each with a ^{13}C shift larger than 30 cm^{-1}, are expected for a species of composition $YXYXY_2$ (X, Y = C, O, or N).[55] We conclude that the pattern of CO stretch modes and associated ^{13}C isotope shifts agree with a surface intermediate of $OCOCO_2^-$ structure and rule out assignment to CO_2^-.

The constant relative intensity of the 1358 and 1346 cm^{-1} pair of bands for ^{12}C (^{13}C: 1326 and 1316 cm^{-1}) is consistent with attribution to a single species although we cannot rule out the possibility that this is fortuitous, i.e. that the pair of bands represents the symmetric stretch of two distinct surface configurations of $OCOCO_2^-$. However, this does not affect our conclusion regarding structural identification as $C_2O_4^-$. Therefore, we assign the bands of the observed one-electron intermediate to surface bound carbon dioxide dimer radical anion of structure Cu-$C(=O)OCO_2^-$. The observed bicarbonate growth is proposed to result from disproportionation upon encounter of $C_2O_4^-$ species (at pH 8, split-off CO_3^{2-} is instantly protonated to bicarbonate).

3.2 Visible light driven CO_2 reduction by aqueous CdSe quantum dots

In search of a photocatalytic CO_2 reduction system that allows us to investigate the relationship between the kinetic behavior of the one-electron intermediate and the CO product, we explored rapid-scan FT-IR spectroscopy of photocatalytic CO_2 reduction on quantized semiconductor chalcogenide nanocrystals such as CdSe.[1,4] Specifically, we used 3-mercaptopropionic acid

(MPA)-capped CdSe quantum dot (~2.4 nm) with Na L-ascorbate (AA) as electron donor. Preliminary tests showed that the efficient $Ni^{I}(TMC)^{+}$ trap for CO remains stable in solution for this system. The AA donor, which is not effective as quencher when using SnP sensitizer but works well for chalcogenide photocatalysts, offers spectroscopic advantages over TEA because of a sparser infrared spectrum. More importantly, the primary oxidation product, dehydroascorbic acid (DHAA) has a characteristic IR absorption at 1795 cm^{-1}, a region free of absorption by any other species. Hence, the rate of electron generation in CdSe particles during photocatalysis can be monitored accurately. When exciting aqueous CdSe in the presence of AA donor (no CO_2 added), DHAA was not observed (Figure S4a) indicating that no H^{+} reduction to H_2 took place (in the absence of electron transfer to protons, excited CdSe particles reduce DHAA back to AA and, hence, DHAA does not accumulate. The reversibility of the AA/DHAA couple in photosensitization experiments is well documented [56]).

In the presence of $Ni^{I}(TMC)^{+}$ trap for the detection of CO, which gives rise to a characteristic infrared absorption of the $[Ni^{I}(TMC)CO]^{+}$ complex at 1967 cm^{-1},[34,37] growth was observed on the tens of s time scale upon photocatalytic CO_2 reduction in aqueous colloidal CdSe solution upon illumination at 405 nm. These experiments were conducted with a transmission infrared liquid cell instead of ATR configuration because the diamond plate does not transmit infrared probe light in the 2300-1900 cm^{-1} window. As can be seen in the FT-IR difference spectra of Figure 6, illumination of the H_2O solution containing 0.1 M AA results in prompt decrease of the absorption of dissolved CO_2 at 2346 cm^{-1} ($^{12}CO_2$, black traces, top; $^{13}CO_2$, 2276 cm^{-1}, blue traces, bottom) under growth of $[Ni^{I}(TMC)^{12}CO]^{+}$ at 1967 cm^{-1}. In the corresponding experiment with $^{13}CO_2$, $[Ni^{I}(TMC)^{13}CO]^{+}$ is detected at 1924 cm^{-1} (Figure 6, bottom traces). The growth of DHAA observed at 1795 cm^{-1} manifests the generation of

separated charges on CdSe particles, with the holes consumed by the AA donor. As in the case of photosensitized CO_2 reduction at Cu nanoparticles, absorption bands emerged at 1360 cm^{-1} ($^{12}CO_2$ runs) and 1330 cm^{-1} ($^{13}CO_2$). Because the $[Ni^{I}(TMC)]^{+}$ species is highly susceptible to oxidation, the oxidized $[Ni^{II}(TMC)]^{2+}$ complex was introduced into the reactant solution, with reduction to active $[Ni^{I}(TMC)]^{+}$ trap species occurring readily upon onset of 405 nm illumination ($Ni^{II/I}$ = -0.65V vs. NHE compared to -1.3 V (NHE) for CdSe Q-dots).[37]

Spectral analysis of the 1360 cm^{-1} (^{12}C) and 1330 cm^{-1} (^{13}C) absorptions detected by rapid-scan ATR FT-IR spectroscopy in H_2O revealed 3 components, as shown in Figure 7a ($^{12}CO_2$ experiment) and Figure 7b ($^{13}CO_2$). The 1361 cm^{-1} (^{12}C, blue trace) and 1327 cm^{-1} components (^{13}C, blue trace) agree well with the symmetric stretch mode of bicarbonate $H^{12}CO_3^-$ and $H^{13}CO_3^-$, respectively (Figure S2). The growth behavior of this species exhibits a clear induction period for the initial tens of s photolysis as shown by the kinetic curve of Figure 7d (blue trace), indicating that it is a secondary photoreduction product. The observation of CO growth (in the form of trapped $[Ni^{I}(TMC)^{12}CO]^{+}$) on the same time scale strongly suggests that bicarbonate is the co-product of CO.

The pair of spectral components with maxima at 1370 and 1336 cm^{-1} (^{12}C) and 1333 and 1297 cm^{-1} (^{13}C) retains their relative intensity during growth (Figure 7a and 7b), consistent with attribution to a single species. In contrast to bicarbonate, this species follows first order growth (Figure 7d, red curve). The 1370/1336 cm^{-1} pair of bands, each with a large ^{13}C isotope shift of 37-39 cm^{-1}, features the same spectral pattern as the symmetric stretch modes of the $C(=O)OCO_2^-$ surface intermediate observed for aqueous Cu nanoparticles. Therefore, we attribute these bands to the $C_2O_4^-$ intermediate on the CdSe nanoparticle surface, with the asymmetric CO stretch absorbing at ~1575 cm^{-1} (^{12}C) and 1547 cm^{-1} (^{13}C) (Figure 7c) (the exact absorption peak of the

asymmetric stretch of Cd-$C_2O_4^-$ is difficult to determine because of spectral overlap with an intense AA absorption at 1588 cm^{-1} (Figures S4). Spontaneous disproportionation of Cd-$C_2O_4^-$ in the dark plays less of a role compared to the Cu catalyst, consistent with the fact that the buildup of the intermediate is substantially smaller for the CdSe system. No spectral change is observed over a period of several minutes after the end of the photocatalysis when AA is used as donor (Figure S5). Most Cd-$C_2O_4^-$ species directly capture a second electron from photoexcited CdSe, resulting in dissociation to CO + CO_3^{2-} followed by protonation to bicarbonate. This mechanism was previously proposed based on electrochemical observations for CO_2 electroreduction at CdS nanocrystals by Yanagida [49] and for photoelectrochemical CO_2 reduction at *p*-InP by Fujishima.[41,57] When using TEA as donor, slow conversion of the intermediate bands to bicarbonate is detected (Figure S6), adding further support for the conclusion that the observed intermediate on CdSe surface is carbon dioxide dimer radical anion as in the case of Cu nanoparticle catalyzed reaction.

4. Discussion

The detection of carbon dioxide dimer radical anion and observation of its kinetic behavior leads to the proposed mechanism for CO_2 reduction at Cu nanoparticle catalyst

$$Cu + 2\,CO_2 + e^- \rightarrow Cu\text{-}C_2O_4^- \qquad (1)$$

$$Cu\text{-}C_2O_4^- + Cu\text{-}C_2O_4^- \rightarrow CO + CO_3^{2-} + 2\,CO_2 + 2\,Cu \qquad (2)$$
$$\downarrow H^+$$
$$HCO_3^-$$

The absence of an induction period for the growth of the Cu-$C_2O_4^-$ species on the time scale of seconds implies that any Cu-CO_2^- intermediate, if formed, grows in and reacts with another CO_2 molecule within 100 ms or faster

$$Cu + CO_2 + e^- \rightarrow Cu\text{-}CO_2^- \qquad (1')$$

$$Cu\text{-}CO_2^- + CO_2 \rightarrow Cu\text{-}C_2O_4^- \qquad (1'')$$

Given the concentration of 0.033 M for CO_2 dissolved in water (1 atm) [58] and assuming a bimolecular rate constant for reaction (1'') of 10^3 L mol^{-1} s^{-1} or higher, which is consistent with electrokinetic observations,[46] the formation of the $C_2O_4^-$ adduct by reactions (1') and (1'') is estimated to be on the tens of millisecond time scale. While the observed kinetic behavior is consistent with adduct formation either by reaction (1") or by transfer of an electron injected into Cu particles directly to surface adsorbed CO_2 in van der Waals contact with one or more adsorbed CO_2 molecules, the latter is the energetically preferred mechanism. Direct electron transfer to a CO_2 dimer to produce Cu-$C_2O_4^-$ intermediate (reaction 1) is estimated to proceed at 0.6 V or more positive potential [57,59] compared to formation of Cu-CO_2^- upon electron transfer to a single CO_2 (reaction (1')). The rate of subsequent conversion of $C_2O_4^-$ to CO and CO_3^{2-} (HCO_3^-) is controlled by the competition between spontaneous bimolecular encounters of Cu-$C_2O_4^-$ species (reaction (2)) and electron delivery by the reduced $SnP^{\cdot-}$ sensitizer to the Cu catalyst particles with bound surface $C_2O_4^-$ intermediate

$$Cu\text{-}C(=O)OCO_2^- + e^- \rightarrow CO + \underset{\downarrow H^+}{CO_3^{2-}} + Cu \qquad (3)$$
$$HCO_3^-$$

Path (2) may involve diffusional collision of different particles, or disproportionation of $C_2O_4^-$ by encounters upon surface diffusion on the same particle.

It is important to note that the detection of the Cu-$C_2O_4^-$ surface intermediate and monitoring of the conversion to 2-electron products CO and bicarbonate is enabled by the one-by-one delivery of electrons of the photosensitized catalysis method. This mode of delivery allows us to tune the time span for converting the $C_2O_4^-$ surface intermediate to 2-electron reduced product and thereby manipulate the concentration buildup and lifetime of the intermediate. While the electrons transferred from $SnP^{\bullet-}$ sensitizer to the Cu particles have well defined potential of -0.87 V corresponding to a modest overpotential of 320 mV for the visible light sensitized conversion $2\ CO_2 + 2\ e^- \rightarrow CO + CO_3^{2-}$ (ε^0=-0.55 V),[57] the absence of a pool of electrons in the metal particle at an applied reducing potential as it exists in the electrocatalytic mode minimizes instant conversion by reaction (3). For electrocatalytically driven experiments, on the other hand, this reaction is fast on the time scale for buildup of surface intermediates, resulting in concentrations too low for spectroscopic detection. In this regard, the CdSe photocatalyzed system offers interesting insights. In contrast to the SnP photosensitized system, delivery of an electron to the Cd-$C(=O)OCO_2^-$ surface intermediate does not require diffusional encounters of the CdSe nanoparticle with sensitizer molecules. Further reduction of the $C_2O_4^-$ surface intermediate only requires photoexcitation of a particle already featuring a surface intermediate

$$\text{Cd-C(=O)OCO}_2^- + e^- \rightarrow \underset{\downarrow\ H^+}{\underset{HCO_3^-}{CO + CO_3^{2-}}} + Cd \qquad (4)$$

The observed induction period for the growth of the 2-electron reduction product clearly demonstrates that a sequential single electron transfer mechanism is operative.

While not the energetically preferred route, the surface density of adsorbed CO_2 molecules influences the extent to which $C_2O_4^-$ formation consists of the sequential steps (1') and (1''). To investigate their role, if any, by direct spectroscopic observation of Cu-CO_2^- (or Cd-CO_2^-) surface intermediate, microsecond or faster time resolution will be required thus precluding methods based on photosensitizers in solution. Also, substantial more signal averaging will be necessary for spectroscopic detection on the faster time scale, rendering systems that use chemical bias in the form of sacrificial reagents less practical. Electrocatalytic approaches using an applied steady state voltage bias superimposed by short voltage pulses of small amplitude, generated by visible light-excited photovoltaic elements for triggering catalysis would provide the required time resolution and repeatability for exploring spectroscopic detection and structural identification of this intermediate and its kinetic behavior.

5. Conclusions

In summary, $C_2O_4^-$ one-electron surface intermediate of CO_2 reduction at aqueous Cu nanoparticle catalyst has been observed by a structure specific spectroscopy for the first time, confirming the recently proposed electrocatalytic mechanism based on Tafel slope analysis.[15] Our rapid-scan FT-IR method revealed a kinetic relationship on the time scale of seconds between the spontaneous decay of the intermediate and the growth of bicarbonate. While the detection of CO coproduct in this temporal window was limited by spectral sensitivity and required recording on longer time scales, photocatalytic CO_2 reduction at aqueous CdSe nanoparticles revealed the direct kinetic link between the one-electron intermediate and CO + HCO_3^- product. Namely, first order growth of $C_2O_4^-$ species accompanied by growth with an

induction period for bicarbonate and CO, the latter in the form of an efficiently trapped Ni complex. The detection of the $C_2O_4^-$ one-electron surface intermediate and elucidation of the kinetic relevancy was made possible by one-by-one delivery of electrons by the photosensitization method, allowing buildup of concentration and extension of the lifetime of the intermediate for detection by rapid-scan FT-IR spectroscopy.

The formation of $C(=O)OCO_2^-$ adduct as one-electron intermediate provides an alternate, lower energy path for the conversion to CO and carbonate compared to CO_2 reduction to CO_2^- generating CO and OH^-. Therefore, CO_2 reduction yields can be improved by enhancing the formation of $C_2O_4^-$ intermediate through an increase of the density of surface adsorbed CO_2 molecules, which at the same time will increase the rate of spontaneous disproportionation of $C_2O_4^-$ because of its higher steady state concentration. This might be achieved by solid nanostructured Cu catalyst supports with selective, high adsorption capacity for CO_2. For example, an approach might be incorporation of Cu nanoparticle catalysts in conducting heterogeneous nanopore environments such as they exist in electron conducting metal organic frameworks [60] that at the same time have a high CO_2 adsorption capacity.[61]

Gaining a molecular-level understanding of elementary steps of CO_2 reduction by determining structure and kinetics of surface intermediates is a key aspect of developing mechanistic understanding. Equally important is the elucidation of accompanying electronic structural changes of surface or subsurface atoms during the catalytic cycle, which requires interrogation by X-ray and electron spectroscopic techniques. The recent discovery of the role of subsurface oxygen atoms during catalytic CO_2 reduction on a Cu electrode in the presence of H_2O by *in situ* ambient pressure XPS illustrates opportunities for unraveling electronic structure dynamics of the catalyst under reaction conditions.[62] Combining what is known about the

electronic structure dynamics of the active metal centers with knowledge of the molecular structural changes of surface intermediates presented here is expected to provide a more detailed mechanistic account for designing heterogeneous catalysts with improved efficiency.

Acknowledgments

This work was supported by the Director, Office of Science, Office of Basic Energy Sciences, Division of Chemical, Geological and Biosciences of the U.S. Department of Energy under Contract No. DE-AC02-05CH11231.

References

[1] White, J. L.; Baruch, M. F.; Pander, J. E.; Hu, Y.; Fortmeyer, I. C.; Park, J. E.; Zhang, T.; Liao, K.; Gu, J.; Yan, Y.; Shaw, T. W.; Abelev, E.; Bocarsly, A. B. *Chem. Rev.* **2015**, 115, 12888-12935.

[2] Costentin, C.; Robert, M.; Saveant, J. M. *Chem. Soc. Rev.* **2013**, *42*, 2423-2436.

[3] Feaster, J. T.; Shi, C.; Cave, E. R.; Hatsukade, T.; Abram, D. N.; Kuhl, K. P.; Hahn, C.; Norskov, J. K.; Jaramillo, T. F. *ACS Catal.* **2017**, *7*, 4822-4827.

[4] Hori, Y. Electrochemical CO_2 reduction on metal electrodes. In *Modern Aspects of Electrochemistry;* Vayenas, C.; White, R.; Gamboa-Aldeco, M., Eds.; Springer: New York, 2008; Vol. 42, pp 89-189.

[5] Gattrell, M.; Gupta, N.; Co, A. *J. Electroanal. Chem.* **2006**, *594*, 1-19.

[6] Hansen, H. A.; Varley, J. B.; Peterson, A. A.; Norskov, J. K. *J. Phys. Chem. Lett.* **2013**, *4*, 388-392.

[7] Schouten, K.; Kwon, Y.; van der Ham, C.; Qin, Z.; Koper, M. T. M. *Chem. Sci.* **2011**, *2*, 1902-1909.

[8] Mariano, R. G.; McKelvey, K.; White, H. S.; Kanan, M. W. *Science* **2017**, *358*, 1187-1192.

[9] Li, C. W.; Ciston, J.; Kanan, M. W. *Nature* **2014**, *508*, 504-507.

[10] Kim, D.; Xie, C.; Becknell, N.; Yu, Y.; Karamad, M.; Chan, K.; Crumlin, E. J.; Norskov, J. K.; Yang, P. *J. Am. Chem. Soc.* **2017**, *139*, 8329-8336.

[11] Clark, E. L.; Hahn, C.; Jaramillo, T. F.; Bell, A. T. *J. Am. Chem. Soc.* **2017**, *139*, 15848-15857.

[12] Kim, D.; Kley, C. S.; Li, Y.; Yang, P. *Proc. Natl. Acad. Sci. U.S.A.* **2017**, *114*, 10560-10565.

[13] Mistry, H.; Varela, A. S.; Bonifacio, C. S.; Zegkinoglou, I.; Sinev, I.; Choi, Y. W.; Kisslinger, K.; Stach, E. A.; Yang, J. C.; Strasser, P.; Roldan Cuenya, B. *Nature Commun.* **2016**, *7*, 12123.

[14] Gurudayal; Bullock, J.; Sranko, D. F.; Towle, C. M.; Lum, Y.; Hettick, M.; Scott, M. C.; Javey, A.; Ager, J. *Energy Environ. Sci.* **2017**, *10*, 2222-2230.

[15] Manthiram, K.; Beberwyck, B. J.; Alivisatos, A. P. *J. Am. Chem. Soc.* **2014**, *136*, 13319-13325.

[16] Wuttig, A.; Yoon, Y.; Ryu, J.; Surendranath, Y. *J. Am. Chem. Soc.* **2017**, *139,* 17109-17113.

[17] Kortlever, R.; Shen, J.; Schouten, K. J. P.; Calle-Vallejo, F.; Koper, M. T. M. *J. Phys. Chem. Lett.* **2015**, *6*, 4073-4082.

[18] Shi, C.; Hansen, H. A.; Lausche, A. C.; Norskov, J. K. *Phys. Chem. Chem. Phys.* **2014**, *16*, 4720-4727.

[19] Goodpaster, J. D.; Bell, A. T.; Head-Gordon, M. *J. Phys. Chem. Lett.* **2016**, *7*, 1471-1477.

[20] Wuttig, A.; Liu, C.; Peng, Q.; Yaguchi, M.; Hendon, C. H.; Motobayashi, K.; Ye, S.; Osawa, M.; Surendranath, Y. *ACS Cent. Sci.* **2016**, *2*, 522-528.

[21] Wuttig, A.; Yaguchi, M.; Motobayashi, K.; Osawa, M.; Surendranath, Y. *Proc. Natl. Acad. Sci. U.S.A.* **2016**, E4585-E4593.

[22] Baruch, M. F.; Pander, J. E.; White, J. L.; Bocarsly, A. B. *ACS Catal.* **2015**, *5*, 3148-3156.

[23] Dunwell, M.; Lu, Q.; Heyes, J. M.; Rosen, J.; Chen, J. G.; Yan, Y.; Jiao, F.; Xu, B.; *J. Am. Chem. Soc.* **2017**, *139*, 3774-3783.

[24] Liu, Y.; Chen, S.; Quan, X.; Yu, H. *J. Am. Chem. Soc.* **2015**, *137*, 11631-11636.

[25] Heyes, J.; Dunwell, M.; Xu, B. *J. Phys. Chem. C* **2016**, *120*, 17334-17341.

[26] Rosen, B. A.; Haan, J. L.; Mukherjee, P.; Braunschweig, B.; Zhu, W.; Salehi-Khojin, A.; Dlott, D. D.; Masel, R. I. *J. Phys. Chem. C* **2012**, *116*, 15307-15312.

[27] Firet, N. J.; Smith, W. A. *ACS Catal.* **2017**, *7*, 606-612.

[28] Zhu, S.; Jiang, B.; Cai, W. B.; Shao, M. *J. Am. Chem. Soc.* **2017**, *139*, 15664-15667.

[29] Figueiredo, M. C.; Ledezma Yanez, I.; Koper, M. T. M. *ACS Catal.* **2016**, *6*, 2382-2392.

[30] Neatu, S.; Macia-Agullo, J. A.; Concepcion, P.; Garcia, H. *J. Am. Chem. Soc.* **2014**, *136*, 15969-15976.

[31] Aldeek, F.; Balan, L.; Lambert, J.; Schneider, R. *Nanotech.* **2008**, *19*, 475401-9.

[32] Yu, W.; Qu, L.; Guo, W.; Peng, X. *Chem. Mater.* **2003**, *15*, 2854-2860.

[33] Kim, W.; Park, J.; Jo, H. J.; Kim, H. J.; Choi, W. *J. Phys. Chem. C* **2008**, *112*, 491-499.

[34] Szalda, D. J.; Fujita, E.; Sanzenbacher, R.; Paulus, H.; Elias, H. *Inorg. Chem.* **1994**, *33*, 5855-5863.

[35] Xiong, J.; Wang, Y.; Xue, Q.; Wu, X. *Green Chem.* **2011**, *13*, 900-904.

[36] Kim, W.; Frei, H. *ACS Catal.* **2015**, *5*, 5627-5635.

[37] Froehlich, J. D.; Kubiak, C. P. *J. Am. Chem. Soc.* **2015**, *137*, 3565-3573.

[38] Kim, W.; Tachikawa, T.; Majima, T.; Li, C.; Kim, H. J.; Choi, W. *Energy Environ. Sci.* **2010**, *3*, 1789-1795.

[39] Bellamy, L. J. *The Infrared Spectra of Complex Molecules, 3rd ed.*; Chapman and Hall: London, Vol. 1, 1975. p. 290.

[40] Davis, A. R.; Oliver, B. G. *J. Solution Chem.* **1972**, *1*, 329-339.

[41] Tryk, D. A.; Yamamoto, T.; Kokubun, M.; Hirota, K.; Hashimoto, K.; Okawa, M.; Fujishima, A. *Appl. Organometal. Chem.* **2001**, *15*, 113-120.

[42] Lamy, E.; Nadjo, L.; Saveant, J. M. *J. Electroanal. Chem.* **1977**, *78*, 403-407.

[43] Hori, Y.; Wakebe, H.; Tsukamoto, T.; Koga, O. *Electrochimica Acta* **1994**, *39*, 1833-1839.

[44] Aylmer-Kelly, A. W. B.; Bewick, A.; Cantrill, P. R.; Tuxford, A. M. *Discuss. Faraday Soc.* **1973**, *56*, 96-107.

[45] Gennaro, A.; Isse, A. A.; Severin, M. G.; Vianello, E. *J. Chem. Soc., Faraday Trans.* **1996**, 92, 3963-3968.

[46] Amatore, C.; Saveant, J. M. *J. Am. Chem. Soc.* **1981**, *103*, 5021-5023.

[47] Amatore, C.; Saveant, J. M. *J. Electroanal. Chem.* **1981**, *126*, 1-19.

[48] Fujiwara, H.; Hosokawa, H.; Murakoshi, K.; Wada, Y.; Yanagida, S. *J. Phys. Chem. B* **1997**, *101*, 8270-8278.

[49] Fujiwara, H.; Hosokawa, H.; Murakoshi, K.; Wada, Y.; Yanagida, S. *Langmuir* **1998**, *14*, 5154-5159.

[50] Freund, H. J.; Roberts, M. W. *Surf. Sci. Rep.* **1996**, *25*, 225-273.

[51] Thompson, W. E.; Jacox, M. E. *J. Chem. Phys.* **1999**, *111*, 4487-4496.

[52] Zhou, M.; Andrews, L. *J. Chem. Phys.* **1999**, *110*, 2414-2422.

[53] Akeman, W.; Otto, A. *Surf. Sci.* **1993**, *287/288*, 104-109.

[54] Wohlrab, S.; Ehrlich, D.; Wambach, J.; Kuhlenbeck, H.; Freund, H. J. *Surf. Sci.* **1989**, *220*, 243-252.

[55] Stirling, A.; Papai, I.; Mink, J.; Salahub, D. R. *J. Chem. Phys.* **1994**, *100*, 2910-2923.

[56] Shan, B.; Baine, T.; Ma, X. A. N.; Zhao, X.; Schmehl, R. H. *Inorg. Chem.* **2013**, *52*, 4853-4859.

[57] Hirota, K.; Tryk, D. A.; Yamamoto, T.; Hashimoto, K.; Okawa, M.; Fujishima, A. *J. Phys. Chem. B* **1998**, *102*, 9834-9843.

[58] *CRC Handbook of Chemistry and Physics 85th ed.;* Lide, D. R., ed.; CRC Press: Boca Raton, 2004. p. 8-91.

[59] Quitevis, E. L.; Herschbach, D. R. *J. Phys. Chem.* **1989**, *93*, 1136-1139.

[60] Lin, S.; Diercks, C. S.; Zhang, Y. B.; Kornienko, N.; Nichols, E. M.; Zhao, Y.; Paris, A. R.; Kim, D.; Yang, P.; Yaghi, O. M.; Chang, C. J. *Science* **2015**, *349*, 1208-1213.

[61] Millward, A. R.; Yaghi, O. M. *J. Am. Chem. Soc.* **2005**, *127*, 17998-17999.

[62] Favaro, M.; Xiao, H.; Cheng, T.; Goddard, W. A.; Yano, J.; Crumlin, E. J. *Proc. Natl. Acad. Sci. U.S.A.* **2017**, *114*, 6706-6711.

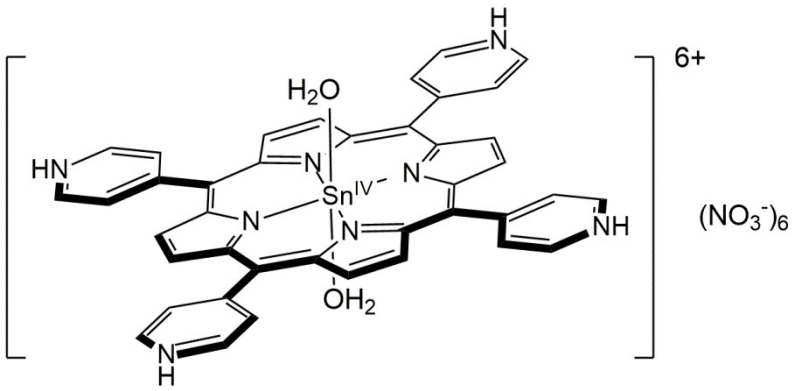

Figure 1: Visible light sensitizer SnP = protonated *trans*-dihydroxo[5,10,15,20-tetra(4-pyridyl)-porphyrinato]tin(IV)

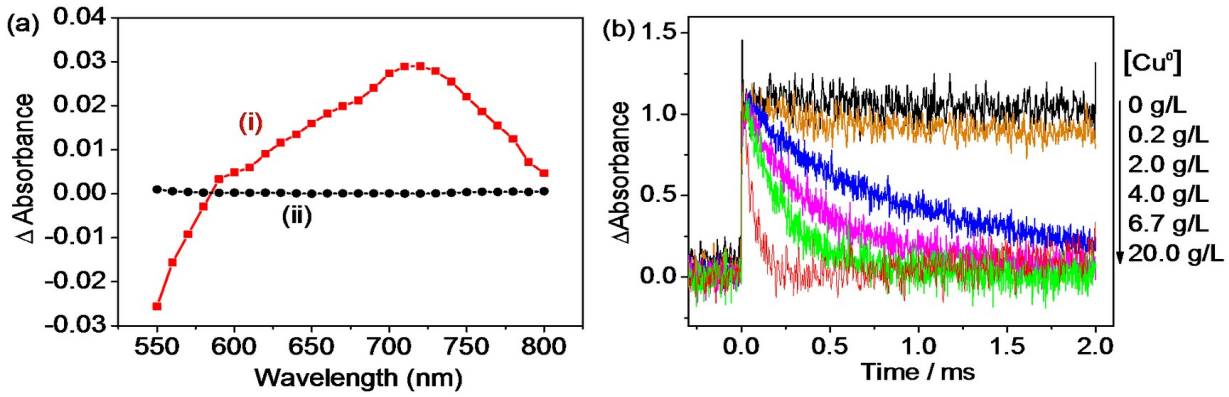

Figure 2: (a) Transient absorption spectra observed at 100 μs after laser excitation at 550 nm (8 ns, 10 mJ/pulse) of SnP (50 μM, aqueous solution) in the presence (trace (i)) or absence (trace (ii)) of 0.3 M TEA electron donor. (b) Decay traces of SnP radical anion recorded at 697 nm in the presence of 0.1 M TEA and Cu nanoparticles at concentrations up to 20 g/L.

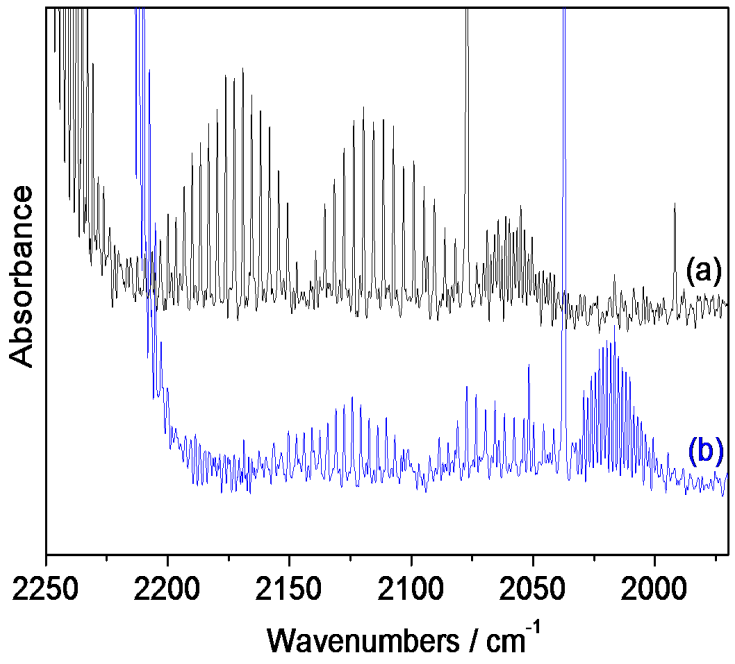

Figure 3: Gas phase FT-IR spectra of (a) ^{12}CO and (b) ^{13}CO product accumulating in the head space upon visible light sensitized carbon dioxide reduction at aqueous Cu nanoparticles recorded at 0.25 cm^{-1} resolution. The rotation-vibration bands below 2154 cm^{-1} ($^{12}CO_2$) and 2075 cm^{-1} ($^{13}CO_2$) are due to $\nu_1+\nu_2$ combination transitions of $^{12}CO_2$ and $^{13}CO_2$, respectively. The strong absorptions onset above 2200 cm^{-1} is due to the intense ν_3 transition of carbon dioxide.

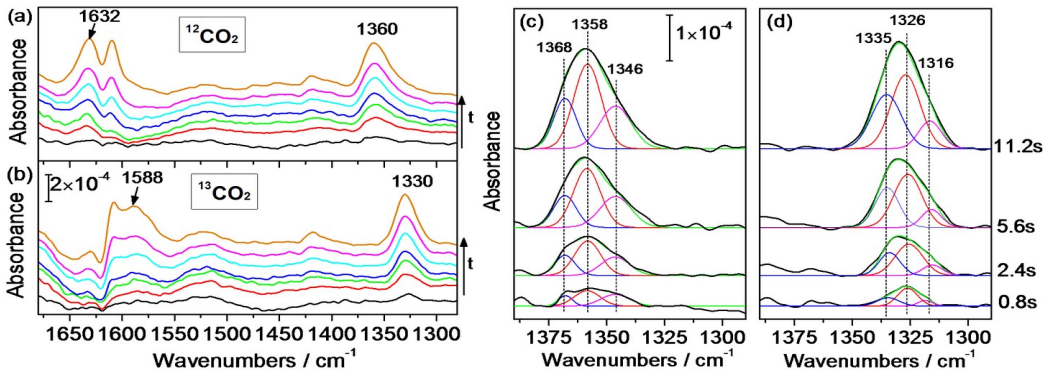

Figure 4: CO_2 reduction at Cu nanoparticles (1.5 g/L) in D_2O upon illumination of SnP sensitizer (SnP (0.1 mM), diethylamine-d_{10} (0.1 M)) at 405 nm. (a) Solution saturated with $^{12}CO_2$. Traces were recorded at 0.8, 2.4, 4.0, 5.6, 8.0, 11.2, 17.6 s (bottom to top). (b) Same experiment with $^{13}CO_2$. (c) and (d) Deconvolution of the infrared bands in the 1380-1300 cm^{-1} region for spectral traces at 0.8, 2.4, 5.6 and 11.2 s shown in panel (a) and panel (b), respectively. All spectra are referenced to the background recorded before start of photosensization.

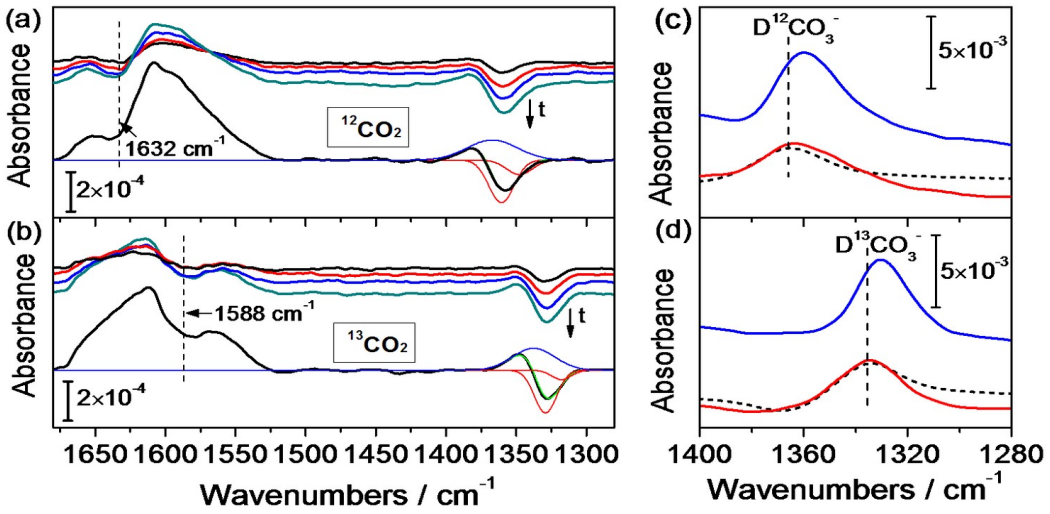

Figure 5: FT-IR spectra of spontaneous reaction under dark conditions following illumination of SnP sensitizer in D_2O solution of Cu nanoparticles. (a) Top: Difference spectra recorded at 12, 20, 30, and 60 s after 405 nm illumination of solution containing $^{12}CO_2$ (top to bottom). Bottom: Deconvolution of difference spectrum after dark period of 136 s showing decreasing $C_2O_4^-$ intermediate bands (red) and growing DCO_3^- (blue). (b) Identical experiment for $^{13}CO_2$ containing sample. (c) Comparison of spectra in the 1400-1280 cm^{-1} region at the end of 405 nm illumination of SnP sensitizer in D_2O solution of Cu nanoparticles and $^{12}CO_2$ (top, blue), and after 136 s dark period (bottom, red). The dotted curve shows authentic spectrum of DCO_3^- generated in the same solution by bubbling of CO_2. (d) Identical experiment with $^{13}CO_2$.

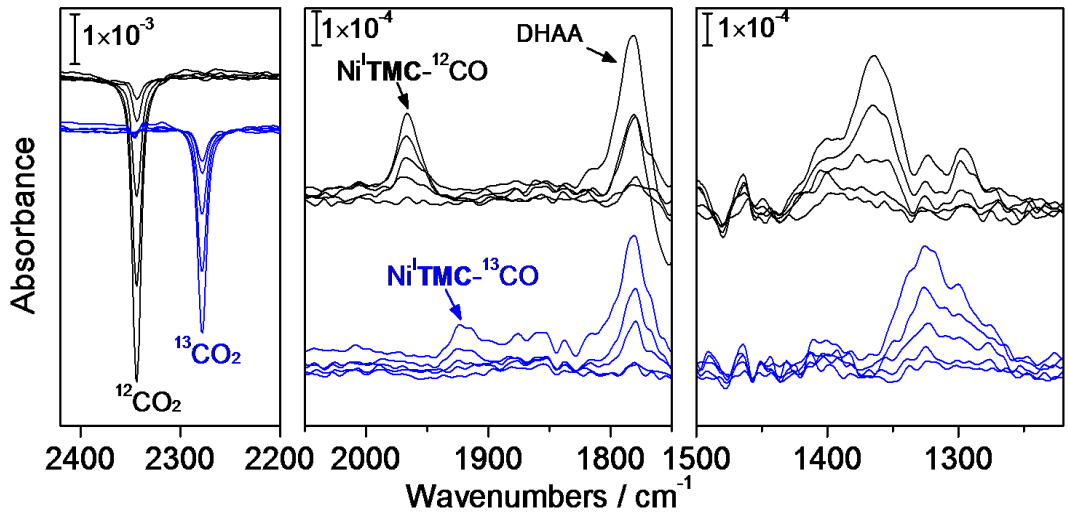

Figure 6: FT-IR spectroscopy of CO_2 reduction at CdSe photocatalyst particles (0.4 mM, AA 0.1 M) in H_2O upon excitation at 405 nm (170 mW) in the presence of $[Ni^{I}TMC]^{+}$ for trapping of CO ($[Ni^{II}\mathbf{TMC}]Cl_2$ (5 mM)). Top, experiments in $^{12}CO_2$ saturated solution (black). Bottom, $^{13}CO_2$ bubbled solution (blue)). A 25 µm CaF_2 liquid cell in transmission mode was used. The 1650-1550 cm^{-1} region is blocked by absorption of the H_2O.

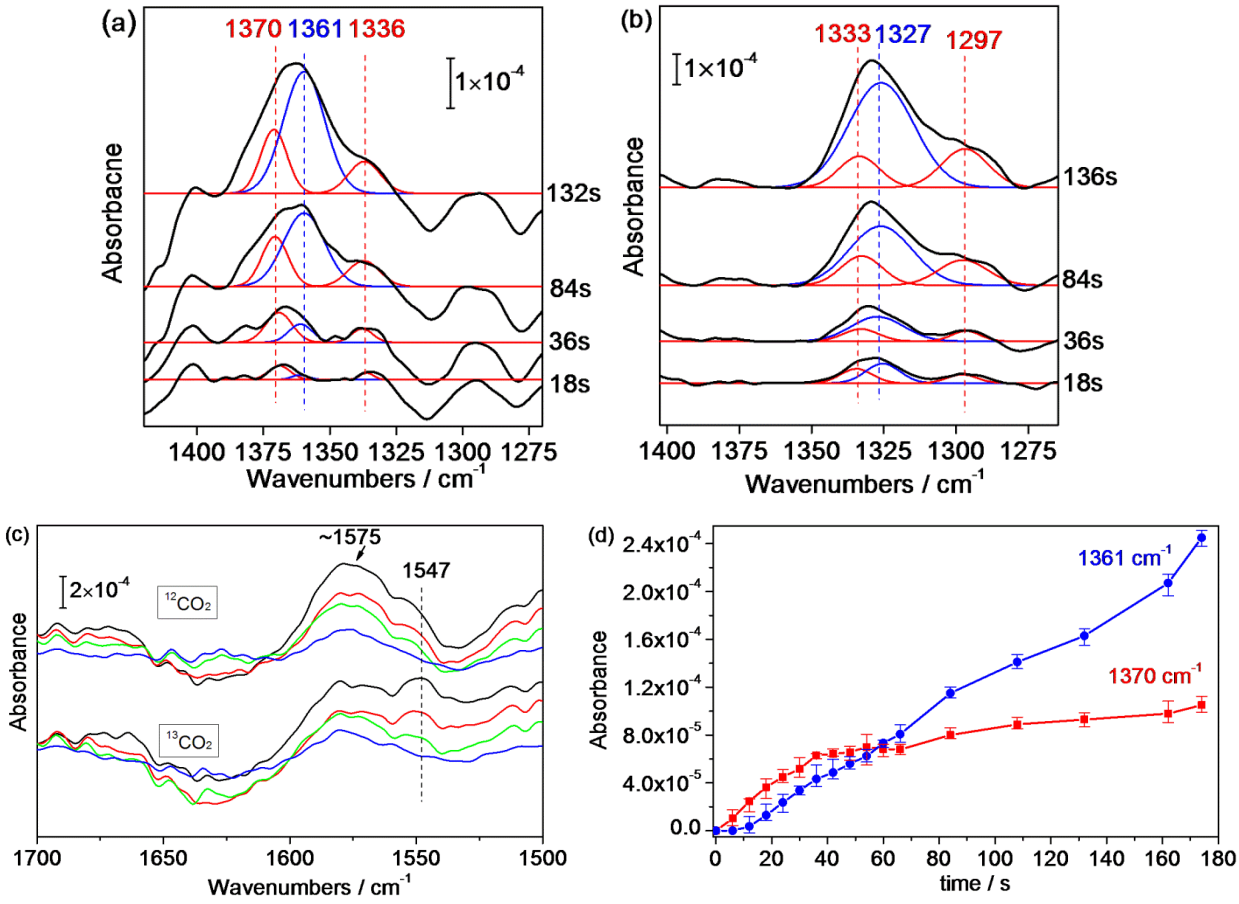

Figure 7: FT-IR spectroscopy in ATR configuration of CO_2 reduction at CdSe photocatalyst particles (0.4 mM, AA 0.1 M) in H_2O (405 nm, 170 mW). (a) Symmetric stretch region of solution saturated with 12CO2. (b) Symmetric stretch region saturated with $^{13}CO_2$. (c) Asymmetric stretch region of $^{12}CO_2$ (top) and $^{13}CO_2$ saturated solution (bottom) showing time slices upon illumination for 18, 36, 84, 136 s. (d) Growth kinetics of CO_2 reduction intermediate (1370 cm^{-1}) and bicarbonate (1361 cm^{-1}) during illumination

TOC Graphics